14,08

Features of defect structure evolution in the discrete element model

© E.E. Damaskinskaya, V.L. Hilarov

Ioffe Institute,
St. Petersburg, Russia

E-mail: Kat.Dama@mail.ioffe.ru

Received October 19, 2023
Revised November 12, 2023
Accepted November 13, 2023

A model of heterogeneous material fracture based on the discrete element method is constructed, which helps to study in detail the evolution of defects and acoustic emission accompanying their formation. It is shown that the analysis of the type of acoustic event amplitude distribution function allows us to determine the moment of time when the defect system transitions to the state of self-organized criticality.

Keywords: computer modeling, discrete element method, defect evolution, acoustic emission event distributions.

DOI: 10.61011/PSS.2024.01.57867.233

1. Introduction

Numerous experiments for deformation of natural heterogeneous materials have found that the accumulation of defects has several stages [1–8]. At the start of loading, randomly distributed defects occur throughout the test material. Then, concentration of defect formation is observed in a particular space, which is the site of fracture development.

To predict the fracture process development and assess the criticality of the strained condition of materials, physical mechanisms governing the defect formation and causes of qualitative transition from disperse (stable) damage accumulation stage to critical (or dangerous) stage shall be understood. A set of studies is devoted to the search of criteria of transition from the random defect accumulation stage to the fracture site formation stage [2,9–13].

We have shown that energy distribution of acoustic emission (AE) signals is not always described by the Gutenberg–Richter relation, i. e. not always can be approximated by the power function. It was found [14] that, at the random defect accumulation stage, AE signal distribution is approximated by the exponential function, while, at the localization (fracture formation) stage, energy distribution of AE signals becomes a power function. We believe that this fact reflects qualitative change in the defect formation mechanism: transition from the Markovian process to the self-organized critical state.

Physical mechanisms of transition between the fracture stages and factors that influence it are still not understood. One of the reasons is in the difficulty of acquisition of reliable experimental data on the defect parameters to be detected in the material directly during loading. Even the state-of-the-art X-ray computer tomography is not capable of achieving the required spatial resolution and, what is particularly important, of examining the sample directly during the strain process.

Therefore, we decided to use computer simulation assuming that the numerical experiments will provide more detailed information for this issue.

Most of the computer models (for example, [15]) used to describe the mechanical behavior of heterogeneous materials are based on the continuum mechanics representations that do not explicitly consider defect formation (discontinuity).

However, to understand physical laws behind defect (fracture) formation and evolution, models based on the discrete element method (DEM) are the most adequate [16,17]. The discrete element model makes it possible to explicitly take into account local discontinuities during deformation, simulating the formation and development of cracks.

The previous study [18] offered a model that adequately describes some features of heterogeneous materials fracture in cases when the main processes take place in the grain boundaries. In particular, realistic loading diagrams are simulated to reflect the equation of state for brittle and ductile materials.

The same model is used herein to study the defects evolution according to the spatial arrangement of bonds broken in various points in time during the sample deformation.

2. Computer experiment description

The computer experiment setup is similar to that described in [18]. Cylindrical samples 10 mm in diameter and (h) 20 mm in height were simulated. The sample was placed into a virtual press. The lower plate was fixed and the upper plate moved downwards at a constant speed of $v = 0.02$ m/s. Thus, uniaxial compression was simulated.

We used the bonded particle model — BPM) that is described in detail in [19]. Various modification of the model are used to study the behavior of materials in the fracture process. Material (rock) model — spherical particles of the same or different sizes simulating the

Table 1. Parameters of materials used for simulation

№	Material	ρ, kg · m^3	E, GPa	ν	σ_n, MPa	σ_t, MPa	η, Pa · s
1	Quartz	2650	94	0.29	600	600	5E19
2	Orthoclase	2560	62	0.29	420	420	1E19
3	Oligoclase	2560	70	0.29	480	480	1E19
4	Quartz-orthoclase bond	2500	5.8	0.2	200	200	5E19
5	Quartz-oligoclase bond	2500	5.8	0.2	300	300	5E19
6	Orthoclase-oligoclase bond	2500	5.8	0.2	100	100	5E19
7	Glass	2500	50	0.22	50	50	1E40

Note. ρ is the material density, E is Young's modulus,ν is Poisson's ratio, σ_n is the tensile strength of the material, σ_t is the shear strength of the material, η is the dynamic viscosity.

Table 2. (Grain diameters (mm) and percentage of each of the grain sizes (samples 1 and 2)

Material	Diameters of various grain sizes d_i, mm					Proportion of each grain size
Quartz	0.09	0.047	0.132	0.079	0.106	0.0595745
Orthoclase	0.068	0.07	0.096	0.91	0.064	0.0702128
Oligoclase	0.041	0.042	0.077	0.063	0.098	0.0702128

Table 3. Grain diameters (mm) and percentage of each of the grain sizes (sample 3)

Material	Diameters of various grain sizes d_i, mm					Proportion of each grain size
Quartz	0.36	0.188	0.52	0.28	0.42	0.0595745
Orthoclase	0.27	0.28	0.4	0.36	0.26	0.0702128
Oligoclase	0.16	0.168	0.288	0.24	0.4	0.0702127

grains and bonds between the particles simulating the grain boundaries. BPM defines crack nucleation as breaking bonds between particles and crack propagation is defined as merging of multiple broken bonds. To get a crack from a set of bonds broken from the beginning of the experiment to a particular point in time, a clustering procedure is required. Thus, defects are hereinafter referred to as the broken bond clusters. Physical and mechanical parameters of the materials that constitute the particles and bonds are listed in Table 1.

The simulation experiments were carried out in MUSEN freeware package [20].

Three types of samples were used for the numerical experiments.

Sample 1 contains the particles with diameters and percentage composition as listed in Table 2 (the number of particles is 33670). This is a set of sizes with a mean value of 0.08 mm and a standard deviation of 0.025 mm which was obtained by a normal random number generator. Grain diameter 4 for orthoclase is increased by an order of magnitude to improve the degree of heterogeneity. There were only orthoclase bonds with a diameter of 0.04 mm.

Sample 2 has the same particle composition as sample 1. The difference is in the bond materials: particles of the same material were bonded by the same material while heterogenous particles were coupled by glass bonds with $d \leq 0.1$ mm.

Sample 3 contains the particles with diameters and percentage composition as listed in Table 3 (the number of particles is 48695). This is a set of sizes with a mean value of 0.3 mm and a standard deviation of 0.1 mm which was obtained by a normal random number generator. Particles of the same material were bonded by the same material while heterogenous particles were coupled by low-modulus bonds 4–6 (Table 1) with $d \leq 0.6$ mm.

Fragments of the sample structure are shown schematically in Figure 1. Different materials are shown by different colors. Spheres — particles, cylinders — bonds.

Thus, sample 1 is more homogenous, sample 2 is similar to a material with brittle low-strength grain boundaries (glass bonds); sample 3 is primarily heterogeneous with respect to the ultimate strength of bonds, bond diameters, and also contains low-modulus bonds capable of elastic deformation.

The experiment finished with failure of the sample (separation into parts). During the experiment, a large set of various mechanical parameters was recorded in equal time periods — data storage interval — to be further used for analysis. This time interval was chosen according to the process stationarity conditions. Positions of the centers

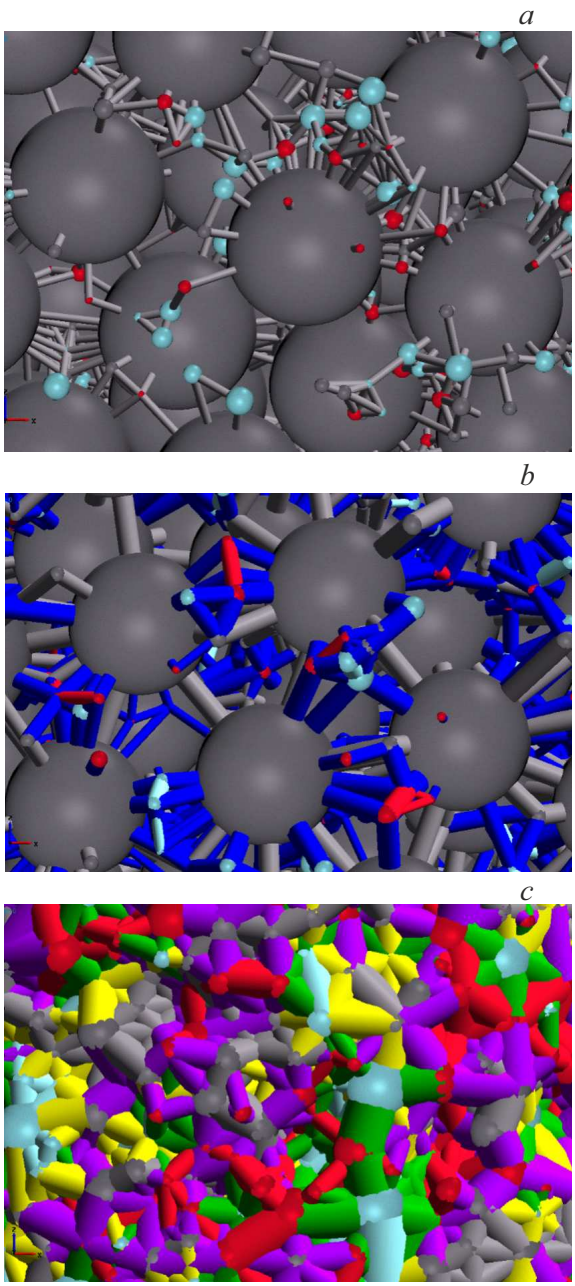

Figure 1. Structure of simulated samples: *a* — sample 1 (all particles have orthoclase bonds); *b* — sample 2 (heterogeneous particles have glass bonds; *c* — sample 3 (heterogeneous particles have low-modulus bonds.) Orthoclase — grey; oligoclase — red; quartz — sky blue; glass — blue; orthoclase-oligoclase bond — violet; quartz-orthoclase bond — yellow; quartz-oligoclase bond — green.

of bonds broken during the sample deformation and bond breakage times were such conditions herein.

Sample loading diagrams are shown in Figure 2. The deformation was calculated using equation $\varepsilon = (v \times t)/h$. The stresses were calculated based on forces acting on the loading plates according to rule described earlier in [18]. In Figure 2, the second horizontal axis corresponds to the experiment time that will be used for further analysis of results.

Stress on sample 1 varies almost linearly up to the maximum value. This sample demonstrates brittle behavior. The loading diagram of sample 2 containing low-strength glass bonds is nonlinear. The curve slope varies within the time interval $t \approx 0.003-0.006$ s. During deformation of sample 3, a linear increase in stress and then an almost horizontal section are observed.

To study the defect evolution and to compare with the laboratory acoustic-emission deformation test data for natural heterogeneous materials, clustering of broken bond centers was carried out. The DBSCAN (density-based spatial clustering of applications with noise [21]) algorithm was used for clustering on the basis of the density of cluster components. The DBSCAN algorithm treats clusters as high-density regions separated by low-density regions. The algorithm includes two parameters, min_samples and eps, that formally define what we imply by density. Higher min_samples or lower eps are indicative of a higher density required for clustering. min_samples is the minimum cluster size; eps is the spatial threshold, i. e. the maximum spacing between the centers of the broken bonds at which clustering is allowable. In our case, min_samples $= 2$, eps $= 0.4$ mm. Such parameters were selected by direct comparison of the clustering data with visually observed clusters. Software for clustering of broken bond centers by the DBSCAN method was developed.

Clustering of bonds broken from the beginning of loading until time t_k provides the picture of defects which have been formed by t_k. For this, the defect size is assumed equal to the number of bonds combined into this cluster.

Clustering of bonds broken during a particular period of time $(t_k; t_k + \Delta t)$ provides an acoustic emission equivalent: each cluster may be treated as an acoustic emission event whose amplitude is equal to the cluster size.

3. Computer simulation data and discussion

Amplitude distribution of acoustic emission events was analyzed to identify the fracture stages. The process was divided into consecutive time intervals whose size was chosen, as described above, according to the process stationarity within each of the intervals. Distributions obtained in each period of time were approximated by exponential and power functions, because these are the functions which a typical for the Markovian process and for the self-organized criticality state. For each approximation, a coefficient of determination R^2 was calculated. Figure 3 shows the variation of the coefficient of determination during deformation. It can be seen that in experiments 1 and 3, there is time t_c until which the coefficient of determination of the exponential function is higher than that of the power function. This means that the distributions are better approximated by the exponential function. For

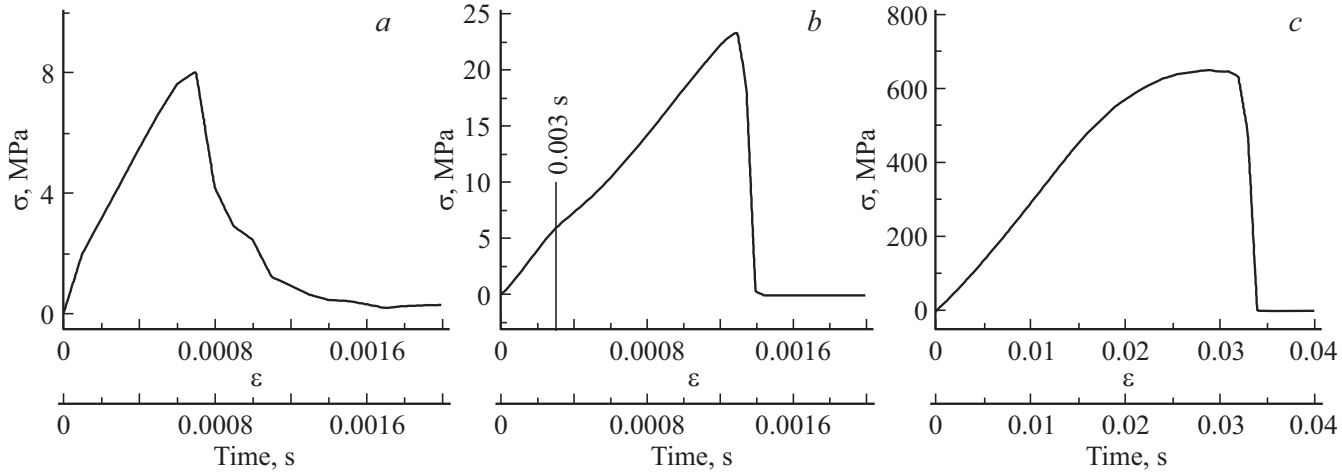

Figure 2. Stress variation in the computer simulation experiment: *a* — sample 1; *b* — sample 2; *c* — sample 3.

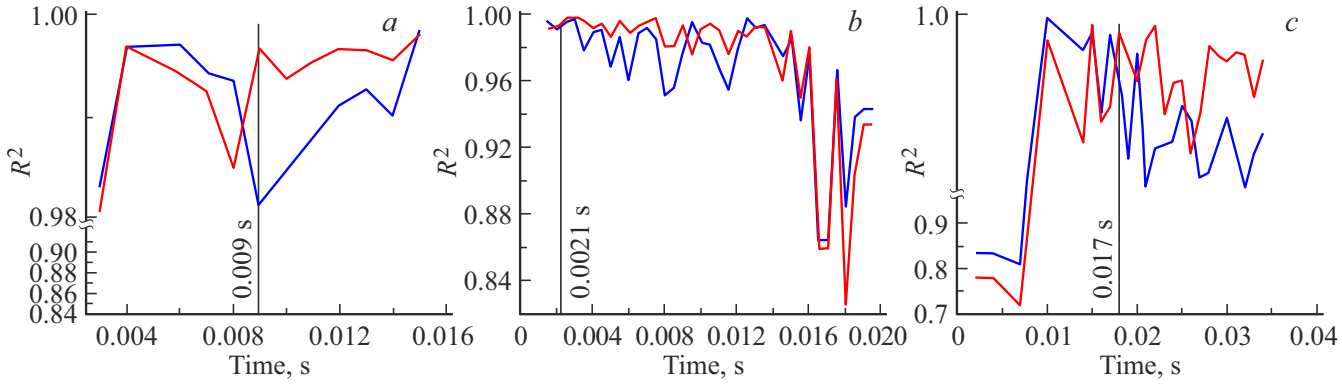

Figure 3. Variation of the coefficient of determination (R^2) during deformation of the samples: *a* — sample 1, *b* — sample 2, *c* — sample 3. Blue line — R^2 approximation with the exponential function, red line — R^2 approximation with power function. Vertical lines indicate the time when the amplitude distribution function of acoustic emission events changes.

sample 1, this moment is 0.009 s, for sample 3, its is — 0.017 s.

Then, beginning from time t_c, event distributions become power-function distributions: coefficient of determination of the power function is higher than that of the exponential function.

Somewhat different picture is observed in loading of sample 2. Here, distribution is exponential in the initial point in time (up to 0.0021 s). Then, almost throughout the experiment, the acoustic emission event amplitude distribution maintains its power-law behavior. Only in the end ($t > 0.18$ s) when sharp decrease in stress occurs, the distribution becomes exponential again.

According to the hypothesis expressed earlier in [14], the type o acoustic emission event distribution function is associated with the defect accumulation behavior.

Figures 4, 5 and 6 show the defects formed in the samples from the beginning of loading to a particular point in time. Pictures typical for the process development stages are shown.

Sample 1. In the beginning of loading, small defects dispersed throughout the sample occur (Figure 4, *a, b*). The size of defects increases gradually. During this time, the acoustic emission event amplitude distribution is exponential. After $t_c = 0.009$ s, fracture localization takes place (Figure 4, *c*) — main crack growth.

Sample 2. The detailed analysis of the acoustic emission event distributions shows that the exponential fashion of the function is observed up to 0.0021 s. During this period, small defects are formed throughout the sample (Figure 5, *a*). Then, within the range of 0.0035–0.006 s, disperse defect formation continues, but the growth of defect sizes is observed (Figure 5, *b, c*). During this period, mainly low-strength glass bonds are broken (Figure 7, *a*) resulting the modulus variation. Restoration of the modulus at $t > 0.006$ s is explained by the fact that in this time the glass bond breaking rate decreases while the breaking rate of other types of bonds is not high enough (Figure 7, *a*). At $t = 0.008$ s, the main crack starts growing (Fiure 5, *d*).

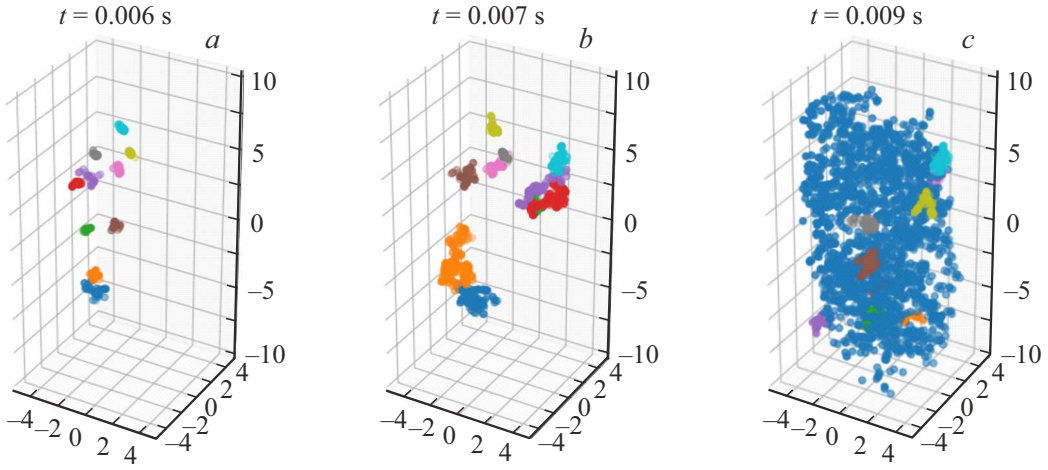

Figure 4. Defect structure evolution in sample 1. Various defects (broken bond clusters) are shown by different colors.

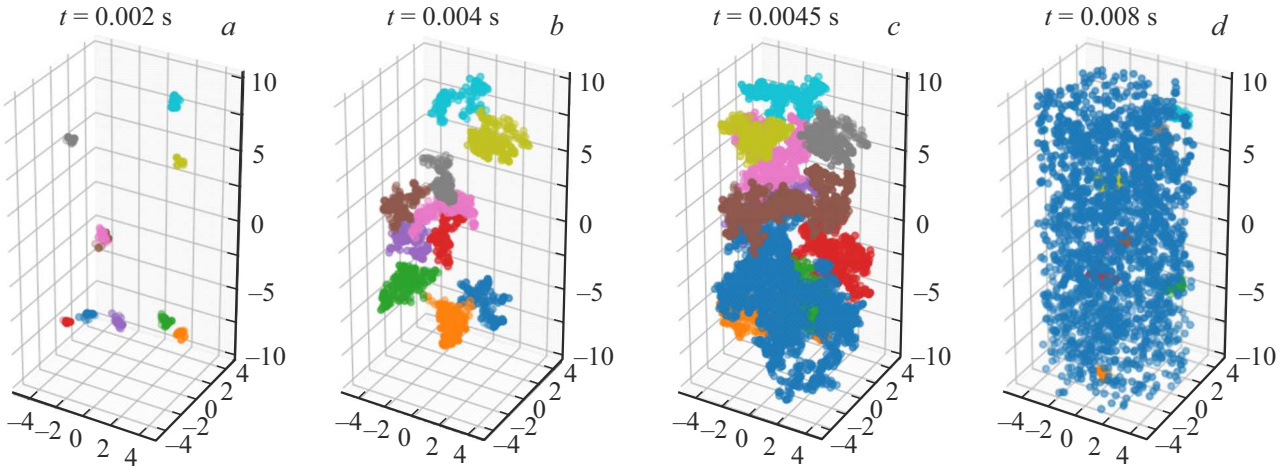

Figure 5. Defect structure evolution in sample 2. Various defects (broken bond clusters) are shown by different colors.

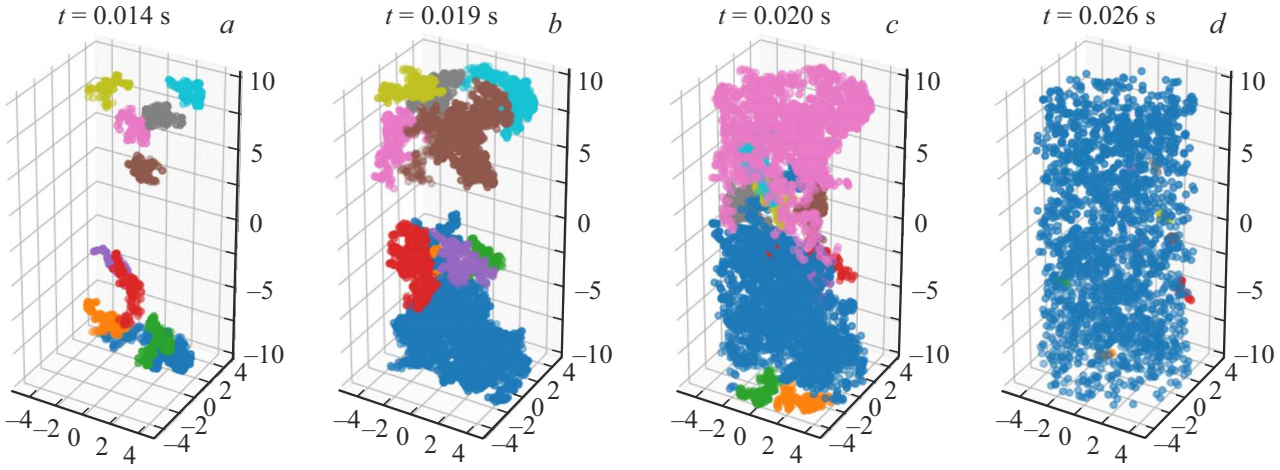

Figure 6. Defect structure evolution in sample 3. Various defects (broken bond clusters) are shown by different colors.

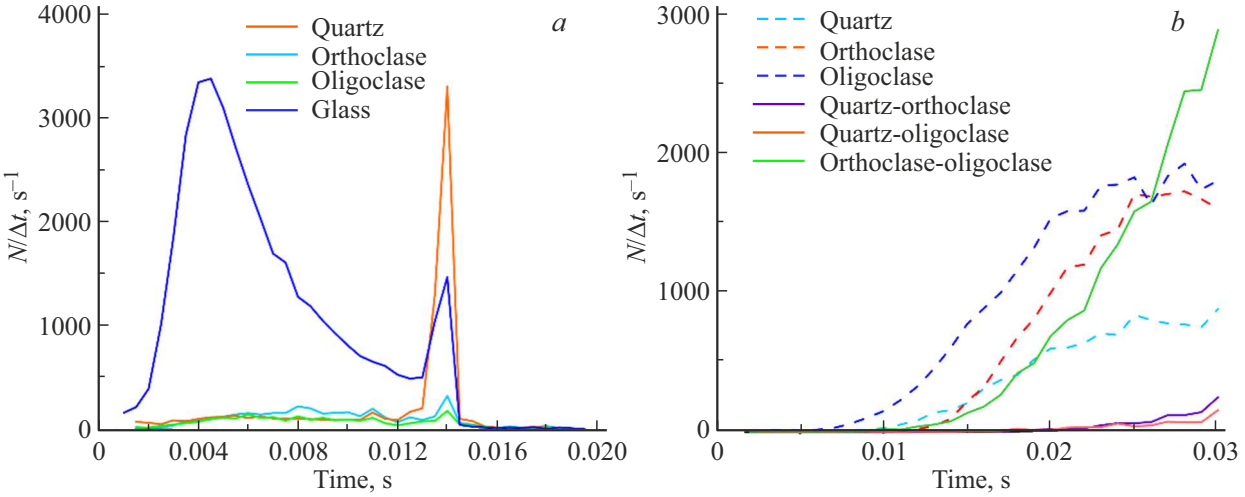

Figure 7. Kinetics of breaking of various types of bonds: *a* — a samples with glass bonds; *b* — a sample with low-modulus bonds.

Sample 3. Before $t_c = 0.017$ s, comparably small defects (about 10) are formed throughout the sample (Figure 6, *a*). Variation of the type of acoustic emission event amplitude distribution function at $t_c = 0.017$ s is associated with the approach to an almost linear section by the loading diagram. Nonlinearity of the loading diagram in this case is explained by the fact that the main contribution to fracture within $0.017 - 0.026$ s is made by high-strength bonds (1–3 from Table 1). Weaker bonds (4–6 rom Table 1) remain primarily intact due to their deformation capability owing to their low modulus of elasticity. Bond breaking kinetics is demonstrated in Figure 7, *b*. In this time range, consolidation of defects dispersed in the sample occurs (Figure 6, *b, c*). Starting from 0.026 s, growth of the main crack is observed (due to primary failure of low-modulus bonds).

4. Conclusion

A computer model was built using the discrete element method to allow detailed investigation of defect formation and development in the fracture process. It is shown that the sample all boundaries of which have orthoclase properties is subjected to brittle fracture by formation of one main crack. While the samples, where glass and low-modulus boundaries exist, show properties similar to plasticity. Advantages of simulation experiments (compared with laboratory experiments) are in the fact that they allowed to compare the evolution pattern of the defect structure and acoustic emission event parameters. Analysis of the acoustic event amplitude distribution made it possible to identify the points in time after which the fracture behavior changes. For the homogeneous sample (all boundaries are orthoclase) — this is the beginning of defect localization (main crack growth). In sample 2 showing a non-linear stress-strain curve, this is the modulus change time associated with the primary breaking of glass bonds. In sample 3 — this is the time when primary fracture of high-strength bonds occurs.

Despite various reasons of the defect formation behavior variation, the power-law type of the acoustic emission event amplitude distributions accompanying the defect formation and growth suggests that the defect system goes into the self-organized critical state.

Conflict of interest

The authors declare that they have no conflict of interest.

References

[1] D.A. Lockner, J.D. Byerlee, V. Kuksenko, A. Ponomarev, A. Sidorin. Nature **350**, 39 (1991).
[2] L.R. Botvina. Fizika Zemli, **10**, 5 (2011). (in Russian).
[3] M. Petružálek, J. Vilhelm, V. Rudajev, T. Lokajíček, T. Svitek. Int. J. Rock Mech. Mining Sci. **60**, 208 (2013).
[4] Y. Hamie, O. Katz, V. Lyakhovsky, Z. Reches, Yu. Fialko. Geophys. J. Int. **167**, 1005 (2006).
[5] V. Kuksenko, N. Tomilin, E. Damaskinskaya, D. Lockner. Pure Appl. Geophys. **146**, *2*, 253 (1996).
[6] V.B. Smirnov, A.V. Ponomarev, P. Bernar, A.V. Patonin. Fizika Zemli, **2**, 17 (2010). (in Russian).
[7] Xinglin Lei, Shengli Ma. Earthq. Sci. **27**, *6*, 627 (2014).
[8] Y. Tal, T. Goebel, J.P Avouac. Earth Planetary Sci. Lett. **536** (2020).
[9] A. Carpinteri, A. Chiodoni, A. Manuello, R. Sandrone. Strain **47**, 282 (2011).
[10] A.V. Ponomarev, A.D. Zavyalov, V.B. Smirnov, D.A. Lockner. Tectonophysics **277**, 57 (1997).
[11] O.B. Naimark. Phys. Mesomech. J. **4**, *4*, 45 (2003).
[12] I.A. Panteleev, O.A. Plekhov, O.B. Naimarik. Fizika Zemli, **6**, 43 (2012). (in Russian).
[13] X. Lei. Appl. Sci. **9**, *12*, 2498 (2019).
[14] E. Damaskinskaya, D. Frolov, D. Gafurova, D. Korost, I. Panteleev. Interpretation **5**, *4*, SP1 (2017).
[15] D. Krajcinovic. Mech Mater. **8**, 117 (1998).

[16] A. Lisjak, G. Grasselli. J. Rock Mech. Geotech. Eng. **6**, 301 (2014).
[17] P.A. Cundall. In: Proc. of the Symposium of Int. Soc. of Rock Mechanics 1. Nancy, France (1971). Paper No. II.
[18] V.L. Hilarov, E.E. Damaskinskaya. FTT **64**, *6*, 676 (2022). (in Russian).
[19] D.O. Potyondy, P.A. Cundall. Int. J. Rock Mech. Min. Sci. **41**, 1329 (2004).
[20] M. Dosta, V. Skorych. Software **X12**, 100618 (2020).
[21] M. Ester, H.-P. Kriegel, J. Sander, X. Xu. In: Proc. of the Second Int. Conf on Knowledge Discovery and Data Mining (KDD-96) / Evangelos Simoudis, Jiawei Han, Usama M. Fayyad. AAAI Press (1996). P. 226.

Translated by E.Ilinskaya